

Development of three-dimensional optimization of a small-scale radial turbine for solar powered Brayton cycle application

Daabo, Ahmed M.; Al Jubori, Ayad; Mahmoud, Saad; Al-dadah, Raya K.

DOI:

[10.1016/j.applthermaleng.2016.09.147](https://doi.org/10.1016/j.applthermaleng.2016.09.147)

License:

Creative Commons: Attribution-NonCommercial-NoDerivs (CC BY-NC-ND)

Document Version

Peer reviewed version

Citation for published version (Harvard):

Daabo, AM, Al Jubori, A, Mahmoud, S & Al-dadah, RK 2017, 'Development of three-dimensional optimization of a small-scale radial turbine for solar powered Brayton cycle application', *Applied Thermal Engineering*, vol. 111, pp. 718-733. <https://doi.org/10.1016/j.applthermaleng.2016.09.147>

[Link to publication on Research at Birmingham portal](#)

Publisher Rights Statement:

Checked 14.11.2016

General rights

Unless a licence is specified above, all rights (including copyright and moral rights) in this document are retained by the authors and/or the copyright holders. The express permission of the copyright holder must be obtained for any use of this material other than for purposes permitted by law.

- Users may freely distribute the URL that is used to identify this publication.
- Users may download and/or print one copy of the publication from the University of Birmingham research portal for the purpose of private study or non-commercial research.
- User may use extracts from the document in line with the concept of 'fair dealing' under the Copyright, Designs and Patents Act 1988 (?)
- Users may not further distribute the material nor use it for the purposes of commercial gain.

Where a licence is displayed above, please note the terms and conditions of the licence govern your use of this document.

When citing, please reference the published version.

Take down policy

While the University of Birmingham exercises care and attention in making items available there are rare occasions when an item has been uploaded in error or has been deemed to be commercially or otherwise sensitive.

If you believe that this is the case for this document, please contact UBIRA@lists.bham.ac.uk providing details and we will remove access to the work immediately and investigate.

Accepted Manuscript

Research Paper

Development of Three-dimensional Optimization of a Small-scale Radial Turbine for Solar Powered Brayton Cycle Application

Ahmed M. Daabo, Ayad Al Jubori, Saad Mahmoud, Raya K. Al-Dadah

PII: S1359-4311(16)31923-8

DOI: <http://dx.doi.org/10.1016/j.applthermaleng.2016.09.147>

Reference: ATE 9172

To appear in: *Applied Thermal Engineering*

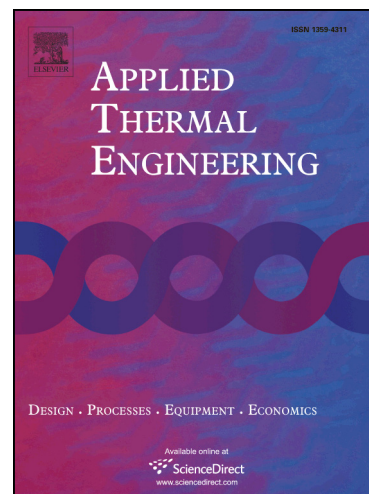
Received Date: 4 July 2016

Revised Date: 30 August 2016

Accepted Date: 25 September 2016

Please cite this article as: A.M. Daabo, A. Al Jubori, S. Mahmoud, R.K. Al-Dadah, Development of Three-dimensional Optimization of a Small-scale Radial Turbine for Solar Powered Brayton Cycle Application, *Applied Thermal Engineering* (2016), doi: <http://dx.doi.org/10.1016/j.applthermaleng.2016.09.147>

This is a PDF file of an unedited manuscript that has been accepted for publication. As a service to our customers we are providing this early version of the manuscript. The manuscript will undergo copyediting, typesetting, and review of the resulting proof before it is published in its final form. Please note that during the production process errors may be discovered which could affect the content, and all legal disclaimers that apply to the journal pertain.



Development of Three-dimensional Optimization of a Small-scale Radial Turbine for Solar Powered Brayton Cycle Application

Ahmed M. Daabo^{a, b*}, Ayad Al Jubori^a, Saad Mahmoud^a, Raya K. Al-Dadah^a

^a The University of Birmingham, School of Engineering,
Edgbaston, Birmingham, B15-2TT, UK

Email: axd434@bham.ac.uk

^b The University of Mosul, Mech. Eng. Dept. Iraq

Abstract

Numerical simulation was carried out to optimize the design of a small-scale radial turbine. One-dimensional (1D) Mean Line (ML) approach and three-dimensional computational fluid dynamic (3D CFD) simulations, using 3D Reynolds-Averaged Navier-Stokes (RANS) models with the shear stress transport (SST) turbulence model in ANSYS@15- CFX, were employed to achieve the best turbine performance and consequently cycle efficiency. For the current study, a new methodology that integrates the Brayton cycle analysis with modelling of a highly efficient small -scale radial turbine at a wide range of inlet temperatures was developed. A multi-objective function was utilized for optimizing the designed radial turbine power in the range of 1.5 to 7.5 kW. This method has been developed in order to find the optimum design, from an aerodynamic point of view. After applying a well-designed range of parameters for both the stator and the rotor, the results demonstrated an excellent improvement in the turbine efficiency from 82.3% to 89.7% for the same range of output power. Moreover, the effect of the turbine inlet temperature, rotational speed and pressure ratio was further studied and presented in this paper. Finally, the overall cycle efficiency showed an excellent improvement of about 6.5% for the current boundary conditions; and it yielded more than 10% with the increase in the inlet temperature and the pressure ratio. Such results highlight the potential and the benefits of the suggested methodology to achieve a high performance (i.e. turbine efficiency and cycle efficiency).

Keywords: Small scale radial turbine, Solar Brayton cycle, CFD analysis, 3D Optimization, Genetic algorithm.

1- Introduction

The demand for energy is continually increasing day after day, but at the same time, investigations around the world into sustainable sources of power are growing in number. Solar energy is considered one of the main renewable energy sources which can play an important role in decreasing CO₂ emissions. It can be efficiently used to generate electricity using different types of thermal power cycles, such as the Brayton cycle.

Moreover, small scale turbines are considered as a promising technology because of their low initial costs, low maintenance, durability and simple construction. Furthermore, they can offer a solution for the power generation demand in domestic or even remote areas. In order to increase the cycle efficiency, one of the main effective ways is to improve the turbines' performance.

Much research has been carried out regarding both the solar Brayton cycle thermodynamic analysis and the selection of the appropriate boundary conditions of energy as heat sources such as [1-4]. For example, an attempt to enhance the overall efficiency of the small-scale solar Brayton cycle, by optimizing both the receiver and the parabolic concentrator, has been achieved by Le Roux et al. [5]. Riazi and Ahmed [6] studied the effect of specific heat ratios for three different working fluids and for air, helium and tetrafluoromethane, on the efficiency of small scale solar energy. A regenerative

48 closed Brayton cycle was analysed in terms of the influence of temperature ratio and the minimum to
49 maximum gas temperature. Their results showed that the higher the specific ratio of the analysed
50 fluid, the higher the cycle efficacy. Moreover, they also suggested that for small-scale Brayton cycles,
51 the performance of lower specific ratios is better as this scale only accumulates a small amount of
52 heat. However, the performance of turbines was not included in all the studies mentioned above as on
53 the shelf turbines were used. Two important parameters have to be carefully considered, as they lead
54 to better preliminary design. Both the loading coefficient and the exit flow coefficient contribute in
55 [7]. Intensive analyses in order to enhance the performance of scroll expander were conducted in [8-
56 10]. Mean line analysis for radial turbines for organic Rankin cycle applications was achieved by
57 many researchers [11-16]. However, no more 84% Total-To-Static efficiency for the studied models
58 of radial turbine have been attained [12]. It is clear that the 3D computational fluid dynamics (CFD)
59 leads to more enhancement in the aerodynamic performance. Three-dimensional optimization design
60 work on ORC radial turbines was demonstrated in [17-19]. On the other hand, modelling and
61 optimization of axial turbines was conducted in [20-21]. Sauret [22] carried out intensively numerical
62 work on a high pressure radial turbine. The author started his study from the preliminary design
63 passing through 3D simulation; then the impact of tip clearance as well as the importance of the
64 diffuser on the turbine's performance was examined at wide range of boundary conditions. The author
65 then validated her design against some experimental data from the literature. Regarding the
66 compressed air radial turbine, it can be seen that only some efforts have been made by different
67 researchers who studied the performance of radial turbines with different design factors as well as
68 boundary conditions. With the aim of identifying the possible acoustic sources which occurs, Marsan
69 and Moreau [23] studied the effect of stator wakes and trailing edge on the impeller blades of radial
70 turbine. In their study the authors showed that the interface regime between the stator and rotor causes
71 pressure fluctuations to the flow passes through these surfaces. They emphasized that the tip clearance
72 losses should not be neglected in analytical studies. Together CFD and FE analysis of relatively high
73 pressure ratio and low inlet temperature, 5 bar and 400 K, radial turbine was conducted in [24]. The
74 output power and efficiency of the investigated turbine were 36.4 and 85% respectively. With
75 comparatively accepted deviation, the authors validated their simulation work using an experimental
76 data. For compressed air turbine optimizations, Tsalicoglou1 and Phillipsen [25] used an iterative
77 method that conducted in-house and commercial CFD codes to decrease the amount of working fluid
78 mass flow rate. This results in changing the turbine blade geometry modifications with some
79 improvement in efficiency. However, with the limitation of the allowed number of design parameters'
80 evaluations, multiple runs were required. As a single objective function, particle swarm optimization
81 was used in their study. An integrated optimization of a 100 kW radial turbine was reported by Lei Fu
82 et al [26]. In their study, an enhancement in terms of aerodynamic and structural performance was
83 achieved. However, the optimization carried out on the rotor while the stator was not considered in
84 their study. Also, each part of optimization was completed separately in two different codes and that
85 might be the reason for the relatively low maximum efficiency value that has been achieved, 82%.
86 Zhang and Ma [27] used the multi-objective algorithm technique for optimizing only the rotor of a
87 radial turbine. Even though the authors claimed the optimized rotor experienced better performance
88 especially in off-design conditions with about an 8% increment in its efficiency, the maximum value
89 that the turbine reached was also low, about 77%.

90 An intensive study on the relation between optimization of computational time and the chosen range
91 of the database, as well as the selection of the suitable optimization method was reported in [28]. In
92 his study the author emphasized that selecting the closer setting to the optimum parameters not only
93 results in further improvements of the convergence, but also contributes to better rotor geometry
94 performance. Three-dimensional multi-objective optimization for a turbocharger radial turbine
95 impeller designed for automotive applications was applied in [29]. With the aim of maximizing its

96 total-to-static efficiency and the impeller moment of inertia, and at the same time keeping mechanical
 97 stresses below a maximum allowable value, the maximum value of efficiency reached was only 80%.

98

99 To the best of the authors' knowledge no work has been published on the 3D multi-objective
 100 optimization of the two main parts of radial turbines: the stator and rotor, together especially for this
 101 scale of turbines. So, this paper tries to focus on design; such as turbine design which creates as high
 102 as possible efficiency and output power to the cycle but with keeping both the rotational speed and the
 103 mass flow rate at their minimum values.

104

105

106 2- Methodology

107

108 In this study the computational fluid dynamic CFD techniques, using ANSYS®15 VISTA, was
 109 utilised in order to first initiate a Mean Line (ML) design for the Small Scale Radial Turbine SSRT
 110 with relatively sufficient performance. Then, 3-D model was improved using ANSYS®15 CFX tool,
 111 which precisely figure out the aerodynamic flow behaviour, analyse were followed in order to have
 112 more accurate and better outcomes for the SSRT. After the best design shape for both the stator and
 113 rotor was achieved, a number of the most influences parameters were determined and chosen with the
 114 aim of optimizing the full blades shape of the SSRT using the 3D Design Exploration feature of
 115 ANSYS®15 which employed the genetic algorithm for the multi-objective optimization. Moreover,
 116 the results have been directly integrated with the Brayton cycle code which was initiated using the
 117 Engineering Equation Solver (EES) software [30].

118

119

120 3- Thermodynamic Analysis of Brayton Cycle

121 The traditional thermal Brayton cycle consists of the compressor, the combustion chamber,
 122 the turbine to extract the air's potential energy and transfer it to mechanical energy; and a pre-heater
 123 to exploit the exhaust energy, which will be otherwise lost to the environment and also to preheat the
 124 cold air before entering the source of heat. However, the solar powered Brayton cycle shown
 125 schematically in Fig. 1, consists of a compressor (1-2), thermal receiver (3-4) and a turbine (4-5). A
 126 recuperator, (2- 3), is used to recover heat from the turbine exit's hot air. The current study aimed to
 127 be fitted with the application of small scale solar powered Brayton cycle which of course its
 128 efficiency can be enhanced by improving the efficiency of its component. The compressor power is
 129 given by [5]:

130

$$130 \quad W_C = \frac{C_p T_1 (R_C K - 1)}{\eta_C} \quad (1)$$

131 Where the compressor pressure ratio equals $R_c = P_2 / P_1$ and in contrast the turbine pressure ratio is:

$$132 \quad R_T = P_4 / P_5$$

133 The amount of heat supply by the solar receiver per unit mass of working fluid flow is:

$$133 \quad Q_{Net} = (T_4 - T_3) \quad (2)$$

134 The heated working fluid exits from the solar receiver and passes through the turbine to generate
 135 power; the power output from the turbine is given by:

$$135 \quad W_T = C_p \eta_T T_4 (1 - R_T - K) \quad (3)$$

136 If the pressure loss coefficient is defined to be X, the above formula can be written as:

$$W_T = Cp \eta_T T_4 (1 - (XR_c) - K) \quad (4)$$

137 The exhaust's working fluid exits from the turbine to the atmosphere and on its way it will pass
138 through the recuperator. The heat gained by incoming compressed air and the heat rejected through
139 the leaving air is given by the next two equations respectively:

$$140 \quad Q_c = \dot{m}(h_2 - h_3) \quad (5)$$

$$Q_{cRej} = \dot{m}(h_5 - h_2) \quad (6)$$

141 The extent to which a recuperator approaches an ideal recuperator is called the effectiveness, ϵ , and is
142 defined as:

$$143 \quad \epsilon = \frac{H_3 - H_2}{H - H_2} \quad (7)$$

144 The net power output from the cycle is given by:

$$W_{net} = W_t - W_c \quad (8)$$

145 This can also be written as:

$$W_{net} = Cp \left[\eta_T T_4 (1 - (XR_c) - K) - \frac{T_1 (R_c K - 1)}{\eta_c} \right] \quad (9)$$

146 The thermal Brayton cycle efficiency is given by:

147

$$\eta_{th} = \frac{W_{net}}{Q_{Net}} \quad (10)$$

148 The above equation can be formulated in terms of temperatures and defined as the following:

149

$$\eta_{th} = \frac{\eta_t T_4 (1 - (XR_c)^{-K}) - T_1 \left(\frac{R_c^{K-1}}{\eta_c} \right)}{T_4 (1 - \epsilon \{1 - \eta_t (1 - (XR_c)^{-K})\}) - T_1 (1 - \epsilon) \left(1 + \left(\frac{R_c^{K-1}}{\eta_c} \right) \right)} \quad (11)$$

150

151

152 As it is shown in Fig. 1 the cycle consists of different components and each one of these
153 component needs to be carefully designed. The selection of the best design parameters of the turbine
154 will lead to higher turbine isentropic efficiency, power output. This certainly will enhance the overall
155 efficiency of the cycle and the system performance. Fig. 2 illustrates their T-S (temperature-entropy)
156 diagram.

157

158 4- Mean Line Design of Radial Turbine [12, 31-41]:

159

160 The initial shape blade as well as its dimensions such as nominal hub and shroud diameters, the
161 blade number and thickness, the trailing and leading edges can be determined using the ML design
162 [41]. Together Figs. 3 & 4 show the velocity triangles and their relative thermodynamic processes. The
163 two dimensionless parameters that have been used in the ML design of radial turbine are the loading
164 (ψ) and flow (ϕ) coefficients. These two parameters are together used to determine the exact velocity
165 triangle shapes and then calculate turbine efficiency through the stage as shown in equations 12-14.

166

$$\psi = \frac{\Delta h_{actual}}{U_4^2} \quad (12)$$

167

$$\phi = \frac{C_{m5}}{U_4} \quad (13)$$

$$\Delta h_{actual} = \Delta h_{isentropic} \eta_{turbine,stage,t5} \quad (14)$$

168 The relations that connect hub and tip diameter in radial turbine as well as the rotor number of vanes

169 are:

$$r_{5t} = \sqrt{\frac{A_5}{\pi}} + r_{5hub}^2 \quad (15)$$

170

$$Z_{rotor} = \frac{\pi}{30} (110 - \alpha_2) \tan(\alpha_2) \quad (16)$$

171

172 The losses in enthalpy due to the tip clearance are consisting of both the axial and radial clearance.

173 So, these clearances as well as the secondary losses are calculated by the next few equations 17- 23,

$$\Delta h_{tip,clearance} = \frac{U_3^4 Z_{rotor}}{8\pi} (0.4 \varepsilon_x C_x + 0.75 \varepsilon_r C_r - 0.3 \sqrt{\varepsilon_x \varepsilon_r C_x C_r}) \quad (17)$$

174

$$C_x = \frac{1 - \left(\frac{r_{5tip}}{r_4}\right)}{C_{m4} b_4} \quad (18)$$

175

$$C_r = \left(\frac{r_{5tip}}{r_4}\right) \frac{l_{rotorx} - b_4}{C_{m5} r_5 b_5} \quad (19)$$

176

$$l_{rotorx} = 1.5(r_{5tip} - r_{5hub}) \quad (20)$$

177

$$\varepsilon_x = \varepsilon_r = 0.04(r_{5tip} - r_{5hub}) \quad (21)$$

178

$$\Delta h_{secondary} = \frac{C_4^2 d_4}{Z_{rotor} r_c} \quad (22)$$

179

$$C_x = \left[\frac{Re}{2} \left(\frac{d_4}{r_c}\right)^2 \right]^{0.05} \left[\frac{W_4 + \left(\frac{W_{5tip} + W_{5hub}}{2}\right)}{2} \right]^2 \frac{l_{hyd}}{h_{hyd}} \quad (23)$$

180 The exit kinetic loss can be computed using the following equation,

181

$$\Delta h_{exit} = 0.5 C_5^2 \quad (24)$$

182

183 In nozzle and volute, on the other hand, after obtaining the friction factor f from moody chart, the

184 differences in the enthalpy because of the friction effect, and Reynolds number can be determined by

185 the next two equations:

$$\Delta h_{friction,nozzle} = 4 f_{nozzle} \bar{C}^2 \frac{l_{hyd,nozzle}}{d_{hyd,nozzle}} \quad (25)$$

$$f = 8 \left[\left(\frac{8}{Re} \right)^{12} + \left(\left[2.475 \ln \left(\frac{1}{\left(\frac{7}{Re} \right)^{0.9} + 0.27PR} \right) \right]^{16} + \left[\frac{37530}{Re} \right]^{16} \right)^{-1.5} \right]^{\frac{1}{12}} \quad (26)$$

186

187

After determining the fluid mass flow rate, its density and absolute velocity, the maximum radius and

188

volute radius can be defined using the equations from 27- 29,

189

$$A_1 = \frac{\dot{m}_{working\ fluid}}{\rho_1 C_1} \quad (27)$$

$$r_{volute} = \sqrt{\frac{A_1}{(0.75\pi + 1)}} \quad (28)$$

190

$$d_{max} = 2(r_1 + r_{volute}) \quad (29)$$

191

192

The losses which are associated with volute geometry and then the total losses in enthalpy and the total to total efficiency are defined in the last three equations:

193

$$\Delta h_{loss,volute} = \frac{r_{volute} C_2^2}{2} \quad (30)$$

194

$$\Delta h_{loss,total} = \Delta h_{loss,volute} + \Delta h_{friction,nozzle} + \Delta h_{tip,clearance}$$

195

$$+ \Delta h_{secondary} + \Delta h_{frictio} + \Delta h_{exit} \quad (31)$$

$$(\eta_{turbine,stage,ts})_{new} = \frac{\Delta h_{actual}}{\Delta h_{actual} + \Delta h_{loss,total}} \quad (32)$$

196

197

The designer can easily get the main specifications and thereby the ML deign of turbines. These specifications, in brief, include Inlet boundary conditions such as pressures, temperature, pressure ratio, and output power as well as design parameters like, flow coefficient, loading coefficients, hub to tip radius ratio and number of blade. Finally, estimation the initial estimations of the overall efficiency initial, tip clearance. Fig. 5 illustrates the main steps of the ML design for the SSRT in a flow chart. Table (1) shows the ranges of input factors and boundary of the radial turbine ML design. The results of the 3D base-line BL of the SSRT geometry from the ML design are shown in Table (2).

198

199

200

201

202

203

5- Numerical Analysis of the model

204

205

206

207

208

209

210

211

212

213

214

Once the ML design of the SSRT, using the Vista RTD tool, was completed, all the relevant information for building the blade geometry of the rotor was prepared. So, the next step was to export these dimensions in order to create the rotor blade geometry using the Blade-Gen feature in ANSYS CFX. This tool in fact can be used to construct the stator blade as well as the rotor for the studied turbine. The CFX Turbo-Grid was employed in order to generate the required elements for the turbine's fluid domain. The 3D turbulent viscous flow simulation in the whole domain of the SSRT was functioned using the Shear Stress Transport turbulence model with equations of Navier-Stokes.

The assumptions of the 3D CFD simulation are steady state, using a compressible single-phase ideal air gas. Also, the first order upwind advection scheme was selected because it is numerically stable. The SST/k-omega has the ability to treat the low velocity region near the wall through an automatic wall function, to capture the turbulence zone by the specified first node after the wall. The SST/K-

215 omega model is specifically designed for the complex flow like turbomachinery flow as suggested by
216 [43]. The flow direction was set to be normal to boundary and the average value of y^+ was set aside
217 unity as recommended in the CFX-Solver theory guide [43]. The convergence criteria for the residuals
218 of the continuity, energy and the velocity equations were of the order of 10^{-6} . The solutions for all the
219 cases were obtained once the results of the convergence criteria were satisfied.

220 The CFD simulations were established in order to analysis the SSRT behaviour at both; the nominal
221 and the other off-design conditions. Figure 6A displays the full SSRT as created by the Blade-Gen
222 CFX; while Fig. 6b presents the density of the chosen mesh passage for the rotor blade. The rotor grid
223 number was about 1,200,000 nodes and the stator grid number was around 600,000 using a finer mesh
224 for the adjacent walls of blades. During the optimization procedure 15 parameters have been
225 nominated in order to achieve the required objective function. Those parameters are: the rotor blade
226 number; the rotor blade shape, which is represented by 12 parameters; the stager angle of the stator;
227 and the stator blade number. More details are found in section 6.

228

229 **6- Validation**

230 Because they have relatively sufficient data, the references [46 & 47] have been chosen and deeply
231 investigated in order to validate the current work. The validation results showed good agreement
232 between the current work and the two chosen ones. While the first validation, which was with
233 reference [46], the CFD technique was used in order to validate the current work, however, in the
234 second validation, with reference [47], only the 1Dimensional approach was used because relatively
235 little information was provided about the 3Dimensional approach. Regarding the mesh sensitivity, it
236 worth to mention that the turbine model had around 1,000,000 nodes for stator and 2,000,000 for the
237 rotor. It is worth noting that in the zone near to the walls and blade's surface, the grid size was refined
238 in order to sustain a good agreement between computational costs and solution accuracy. The grid
239 sensitivity analysis was carried out based on turbine total to static efficiency as shown in Fig. 8 in
240 order to reach the satisfied number of elements for the chosen mesh type.

241

242 The schematic view of the radial turbine that used in Ref [47] is presented in Fig. 7.

243

244 Furthermore, Figs. 9A and B showed the comparison between the present work and the two mentioned
245 journals respectively.

246

247 The authors referred to the secondary losses of the stator, friction losses of the vaneless-space surface,
248 and the mixing trailing edge and wake losses as reasons for the uncertainty of their results. However,
249 the uncertainty of Ref.[45] was because of the difference in the operating conditions of their rig;
250 especially regarding the hot and normal clearances of the rotor, which increases the tip clearance
251 losses.

252 **7- Results of the Base-line Design**

253 Figure 10 compares the CFD results of the base-line design against the ML design analysis at nominal
254 boundary conditions, shown in Table (1). The values of output power and isentropic efficiency were
255 compared for three different cases: inlet temperature, rotational speed and pressure ratio. Specifically,
256 Figs. 10A and 10A' show the values of output power and efficiency at different values of turbine inlet
257 temperatures. In this figure the relative over estimation for the ML analysis in terms of both the
258 turbine output power and the efficiency can be noticed. The main reason for this is the inability of the
259 1D analysis to elicit the exact behaviour of the fluid. Similarly, Figs. 10B, 10B', 10C and 10' represent
260 the turbine output power and efficiency at different values of its rotational speed and pressure ratio
261 respectively. It can be seen that at each specific boundary condition the output power and efficiency
262 of the turbine reached the peak. Furthermore, this figure shows that the maximum difference in

263 efficiency between the PD and CFD results was about 9% for the case of different inlet temperatures
264 and 6.9% in output power for the case of different pressure ratios because the ML design is not able to
265 capture all properties that the real flow behaves.

266 **8- Multi-objective Optimization and Genetic Algorithm**

267 Engineers still need to search for the best design among the available possible designs. Yet, the term
268 ‘best’ can come with many meanings and what is excellent in some terms or applications may not be
269 the best in other applications; thereby this term does not have an absolute meaning. Therefore,
270 understanding the optimization procedure in depth will certainly lay the groundwork for optimization
271 of the turbines; especially the Small Scale Turbines (S.S.T.) whose sizes might add to the challenge of
272 their optimization. The term fitness in nature can be represented, from the engineering point of view,
273 as the most robust design. From this point the idea of initiating an Optimized Small Scale Radial
274 Turbine (O.S.S.R.T.) began and is presented in this paper. The operation of the GA starts with a
275 population of random strings and the design variables are represented by these strings. Thereafter,
276 each single string will be assessed to discover the fitness value. Three main well-known operators –
277 reproduction, cross over, and mutation will be run to create a new population of points and then drive
278 the population. The new population will be further assessed and tested in order to terminate the
279 process. However, if the termination criterion is not met, the population will iteratively run using the
280 three mentioned operators and again be evaluated. This procedure will be continued until the
281 termination criterion is reached. The structure of the algorithm is shown in Fig. 11. In this study the
282 objectives include the efficiency, the power output of the turbine, the mass flow rate of the working
283 fluid and the rotational speed. On the other hand, some constraints such as the stator throat area (to
284 deliver the required mass flow rate of air to the rotor), the tip clearance and blade thickness (for
285 manufactural purposes), are also provided.

286 In this study the multi-objective function was harnessed with the aim of optimizing the designed
287 radial turbine.

288 Comparing it to single objective optimization, the multi-objective has the ability to maximize or
289 minimize many functions, depending on their constraints, simultaneously.

290

291 Differences between the Genetic Algorithm (GA) methods and other traditional optimization
292 methods:

293 1- Genetic algorithms (GA) work with the coding of the parameter set, not the parameters themselves.

294 2- GAs search for a population of points, not a single point.

295 3- GAs use the objective function information and not the derivative or second derivative.

296 4- GAs use stochastic transition rules, not deterministic rules.

297

298 **8.1- Aerodynamic Optimization of SSRT**

299 The design exploration package, which is linked in the CFD analysis, is based on the quadratic
300 Response Surface Method (RSM). This method is one of three popular techniques (Kriging, Radial
301 Basis Functions and polynomial Response Surface Model) in surrogate models. This method, which
302 has the best compromise between the computational expense and modelling accuracy, is provided
303 with a polynomial model. In this study, parameterization of the blade geometry and generation of the
304 design points, using the Design of Experiments (DoE) and design of exploration package in
305 ANSYS®15 was carried out. As the multi-objective optimization enables user to choose more than
306 one objective, each; power output and total efficiency of the turbine together with mass flow rate and
307 rotational speed were chosen as objective functions. Then, the response surface approximation (RSA)

308 [41], which is a statistical functions that connects the output parameters in terms of input parameters
 309 (blade profile), will be employed using ANSYS®15. The GA is employed for global exploration.
 310 After completing the numerical solution for each single design point, the discrete response for each of
 311 them was obtained. The second order polynomial response can be formulated [44, 45] as:

$$f(x) = \beta_0 + \sum_{j=1}^N \beta_j x_j + \sum_{j=1}^N \beta_{jj} x_j^2 + \sum_{i \neq j}^N \sum_{i=1}^N \beta_{ij} x_i x_j \quad (33)$$

312 Here, $f(x)$ is the function to be optimized; β characterizes regression coefficients; and x point to a set
 313 of the design parameters. However, in a constrained minimization problem, the objective function is
 314 replaced by the penalized function which is as follows:

$$P(x) = f(x) + \sum_{j=1}^N u_j (g(x_j))^2 + v_k \sum_{k=1}^K [h_k(x)]^2 \quad (34)$$

315 Where u_j and v_k are penalty coefficients, which are usually kept constant throughout the GA
 316 simulation. The inequality constraints and equality constraints are $g(x)$ and $h(x)$ respectively.
 317 However the fitness function, in terms of a penalized function is as follows:

$$F(x) = \frac{1}{(1 + P(x))} \quad (35)$$

318
 319 If the RSA function is intensively in variation with the design parameters, this leads to redesigning the
 320 space sample between the design points and a rebuilt objective function [43]. The main target of the
 321 current 3D optimization is to enhance the blade geometry in order to minimize the losses through the
 322 passage, in terms of entropy generation; maximize the SSRT efficiency, as well as minimize both the
 323 mass flow rate of the working fluid and the rotor rotational speed. Fig. 12 explains the procedure
 324 followed during the 3D CFD optimization.

325 Both parameterization of the blade geometry and choosing the correct range of the parameters are
 326 considered very important and critical steps in a successful optimization procedure. Therefore, they
 327 need to be carefully selected in order to achieve the requested goal of optimization. Both; the rotor
 328 and the stator blade geometries were conducted in the 3D CFD optimization. Unlike the axial rotor
 329 blade (the airfoil), the rotor blade geometry is presented via a camber line and layered surface because
 330 of its high curvature and the difficulty in representing the exact blade shape using two or three points.
 331 As a result, besides the rotor blade number, twelve other parameters, (some of them in terms of the X
 332 and Y coordinates), which together represent the rotor blade shape and required throat width, have
 333 been selected as input parameters. By doing so, the full definition of the rotor blade will be figured
 334 out. Regarding the stator geometry, there are only two parameters which have been chosen. The first
 335 is the stagger angle which has a direct impact on the stator shape. The second parameter was chosen
 336 to be a constraint objective in order to deliver the same constant mass flow rate to the rotor during the
 337 optimization process.

338 In order to successfully achieve the optimum design for the SSRT, the optimization process was
 339 implemented for the range of design boundary conditions shown in Table (1). The blade shape
 340 parameterization is one of the fundamental aspects of a reliable optimization procedure, as it requires
 341 generating wide ranges of acceptable blade geometry within groups of design variables and their
 342 ranges. The parameterization of the blade's geometry was mainly accomplished for the rotor and only
 343 the stator's stagger angle was included. In addition, the stator's blade number (for constrained mass
 344 flow rate) was defined as a constraint function. Moreover, three different objectives were nominated
 345 as objective functions. Maximizing both the output power and the turbine efficiency were two of the

346 three selected; and minimizing the rotor rotational speed was also desired as the third objective
347 function in the MOGA.

348 8.2- Results of Optimization

349 After defining the parameters, the constraints and the objective functions, more than 1200 different
350 design points (proposed solutions) have been initiated depending on random distributed data. The
351 solution took more than 504 continuous hours on the Core I7 3.7 GHz processor and 48 GB RAM
352 Computer. Figs. 13 A, B and C show an example of some proposed solutions as candidate design
353 points. Due to the large number of them, the design points have been separated into three Figs., (A) to
354 (C). Each one has about 250 proposed solutions (which together represent only about 63% of all the
355 design points) in terms of the output power and the turbine efficiency. From the mentioned figures
356 one can see that some candidate points have about 92% turbine efficiency and even higher efficiency
357 than the chosen optimum point. However, because they didn't satisfy the minimum rotational speed
358 objective, these design points have been omitted. Another important issue that can be concluded from
359 these figures is that not all the candidate points can deliver satisfactory results and come up with a
360 solution. It can be seen that some of them are unable to do so. Table (5) presents the optimum and the
361 base-line values of design variables of turbine, while Fig. 14 displays the two shapes of blade; for the
362 base-line and the design.
363

364 Figure 15 compares the CFD results of the base-line (CFD- Base) design against the Optimum Point
365 (OP) analysis at nominal and off design boundary conditions. The values of the output power and
366 isentropic efficiency were compared for: inlet temperature, rotational speed and pressure ratio.
367 Specifically, Figs. 15A & 15A' show the values of output power and efficiency at different values of
368 turbine inlet temperature. In this figure the effect of the turbine inlet temperature (fixing all other
369 BCs) is highlighted. While there is a positive relationship between the turbine output power and the
370 inlet temperature, the efficiency reached its maximum point at 450K, as it was the designed point.
371 Similarly, Figs. 15B & 15B' and 15C & 15C' represent the turbine output power and efficiency at
372 different values of its rotational speed and pressure ratio respectively. Furthermore, this figure shows
373 that the turbine efficiency and power output increased with a maximum improvement of about 9.35%
374 in turbine efficiency and 41.08% in power output. The main reason behind this enhancement relates to
375 the amount of losses (such as shock losses, secondary losses and incidence losses) that are largely
376 decreased when the blade shape reached its optimum configuration. Moreover, it is obvious from Fig.
377 15 that even in the off-design condition the overall performance of the optimized SSRT is by far
378 better than their peers at the BL for the all investigated boundary conditions. Overall, in its optimum
379 design, the turbine behaves better than the CFD- Base design during the off design conditions
380 especially in terms of the amount of output power.
381

382 Fig. 16A demonstrates the loading distribution (represented in terms of pressure distribution) through
383 all the passage of the rotor. The highest velocity of the flow, which is located at the throat area, results
384 in lowest values of pressure on the suction surface. However, the opposite is the case for velocity
385 distribution on the pressure side starting from the leading to the trailing edges. In Fig. 15B, the
386 contours of pressure distribution through all of the turbine passage, stator and rotor, are presented.
387 From this figure it can be seen how the pressure is distributed starting from the highest value in the
388 stator to the lowest at the diffuser.

389 However, the loss through the rotor passage can be assessed by entropy generation which is an
390 indicator of the amount of aerodynamic losses. From Fig. 17 it is shown that the 3D optimization
391 which is done using the MOGA, was able to decrease the amount of entropy generated within mainly

392 the rotor blade, but also in the stator blade passage, compared to the base-line design and thereby
393 enhance the flow aerodynamically.

394 **9- Results of Brayton Cycle Analysis**

395
396 Using the Brayton cycle analysis in equations 1-11 to calculate the cycle efficiency for the various
397 boundary conditions, the cycle efficiency at nominal and other boundary conditions, as well as the
398 enhancement that the cycle has achieved is clear in Fig. 18. These improvements are delivered by 3D
399 CFD results and inserted in the cycle modelling as inputs to calculate the overall cycle efficiency. This
400 improvement, which is not constant for all the investigated boundary conditions, is mainly due to the
401 increment that occurred in the turbine efficiency. The pressure ratio and inlet temperature values range
402 from 2- 4 and 450 K- 550 K shown in Figs. 18A, B and C respectively. At this point it is worth
403 mentioning that for the nominal conditions, the optimum pressure value that gives maximum cycle
404 efficiency is 3. However, with increasing the turbine inlet temperature the optimum pressure values
405 become 3.5 and 4 at 500 K and 550 K respectively. This is because of the fixed relationship between
406 the turbine inlet temperature and the turbine working pressure ratio. Moreover, for the other boundary
407 conditions of the cycle, with improving the turbine efficiency from about 82% to 89.5 %, the
408 improvement was about 6% at the current nominal conditions, and 5% and 4% at the three investigated
409 temperatures respectively. Finally, it can be seen that the maximum efficiency values which were
410 achieved were about 11%, 18.5% and 27% at the mentioned optimum values of the pressure ratio and
411 for the three inlet temperatures respectively.

412

413 **10- Conclusions**

414 Numerical simulation was carried out to optimize a small-scale radial turbine with output power in the
415 range of 1.5 to 7.5 kW. A one-dimensional Mean Line approach and three-dimensional CFD
416 simulations, using three-dimensional RANS with the SST turbulence model in ANSYS@15- CFX,
417 were employed to achieve the best turbine performance; and consequently, the highest reachable
418 efficiency for the small-scale solar powered Brayton cycle. This paper demonstrated the following
419 important outcomes:

420

- 421 • The CFD simulation results show good agreement with mean line design results for turbine
422 efficiency and power output.
- 423 • A relatively high increment in the isentropic efficiency, from 82.3% to 89.7% for the same
424 range of output power was achieved. This was reached by optimizing the shape and the
425 number of both the stator and the rotor components of the radial turbine.
- 426 • The results showed that a small-scale radial turbine can achieve a power output of around 3.5
427 kW with isentropic efficiency about 89.5% at a relatively low inlet temperature; which can be
428 obtained from solar energy through a parabolic concentrator dish as a heat source.
- 429 • It was clear from the 3D CFD optimization results that the MOGA optimizer is considerably
430 beneficial in improving the turbine's performance in terms of both the turbine efficiency and
431 the power output. Consequently, the thermal cycle efficiency has also been increased by about
432 6% as a result of increasing the turbine's efficiency.
- 433 • Also, the blade loading and losses (entropy generation) had significantly improved compared
434 to the base-line design. So, it can be said that the integrated approach between Brayton cycle
435 modelling, PD, 3D CFD simulation and optimization methodologies have potential
436 advantages to achieve a high performance of a small-scale solar powered Brayton system.

437

438 The integrated aerodynamic and structural optimization is the next study in order to figure out the
 439 mechanical stresses that accompanied the turbine structure during its service.

440 ACKNOWLEDGMENT

441 The author thanks the Higher Committee of Developing Education in Iraq HCED for funding this
 442 project.

443 Nomenclature

Symbol	Definition
A	Area (m ²)
b	Axial chord (mm), blade width (mm)
c	Absolute velocity (m/s)
d	Diameter (m)
f	Friction factor (-)
h	Enthalpy (J/kg)
H	Blade height (mm)
i	Incident angle (deg.)
k	Loss Coefficient (-)
l	Length (m)
m	Mass flow rate (kg/s)
p	Pressure (Pa)
PR	Pressure ratio (-)
r	Radius (m)
Re	Reynolds No. (-)
s	Entropy (J/kg. K)
SC	Swirl coefficient (-)
T	Temperature (K)
U	Rotor blade velocity (m/s)
w	Relative velocity (m/s)
W	Power (W)
Z	Blade number in radial turbine (-)
Greek symbols	Definition
α	Absolute flow angle (deg.)
β	Relative flow angle (deg.)
ε	Clearance (m)
η	Efficiency (%)
υ	Velocity ratio (-)
ρ	Density (kg/m ³)
ϕ	Flow coefficient (-)
ψ	Loading coefficient (-)
ω	acentric factor (-)
ζ	Losses (-)
Acronyms	Definition
BL	Base-line Design
BCs	Boundary Conditions
CFD	Computational Fluid Dynamics
DoE	Design of Experiment
GA	Genetic Algorithm
LE	Leading edge
ML	Mean Line Design
MOGA	Multi-objective genetic algorithm
ORC	Organic Rankine Cycle
O.S.S.R.T	Optimized Small Scale Radial Turbine
RANS	Reynolds-Averaged Navier-Stokes
RSA	Response Surface Approximation
SST	Shear Stress Transport
TE	Trailing Edge
Subscripts	Definition
1-6	Station
m	Meridional direction
r	radial
rel	relative
s	Isentropic
x	Axial

t	Total, stagnation
ts	Total to static
th	Thermal
θ	Tangential/circumferential direction

444

445

446 **References**

- 447 [1] Ordóñez, Juan Carlos, and Adrian Bejan. "Entropy generation minimizations in parallel-plates counter flow
448 heat exchangers." *International Journal of Energy Research* 24.10 (2000): 843-864.
- 449 [2] Le Roux, Willem Gabriel, Tunde Bello-Ochende, and Josua P. Meyer. "Operating conditions of an open and
450 direct solar thermal Brayton cycle with optimised cavity receiver and recuperator." *Energy* 36.10 (2011): 6027-
451 6036.
- 452 [3] Wu, Yuting, et al. "Dynamic simulation of closed Brayton cycle solar thermal power
453 system." *ICSETN2004* (2004): 1-6.
- 454 [4] Le Roux, Willem Gabriel, Tunde Bello-Ochende, and Josua P. Meyer. "Optimum performance of the small-
455 scale open and direct solar thermal Brayton cycle at various environmental conditions and
456 constraints." *Energy* 46.1 (2012): 42-50.
- 457 [5] Le Roux, Willem Gabriel, Tunde Bello-Ochende, and Josua P. Meyer. "The efficiency of an open-cavity
458 tubular solar receiver for a small-scale solar thermal Brayton cycle." *Energy Conversion and Management* 84
459 (2014): 457-470.
- 460 [6] Riazi, H., and N. A. Ahmed. "Effect of the ratio of specific heats on a small scale solar Brayton
461 cycle." *Procedia Engineering* 49 (2012): 263-270.
- 462 [7] Chen, H., and N. C. Baines. "The aerodynamic loading of radial and mixed-flow turbines." *International
463 journal of mechanical sciences* 36.1 (1994): 63-79.
- 464 [8] Collings, Peter, and Zhibin Yu. "Modelling and analysis of a small-scale Organic Rankine Cycle system with
465 a scroll expander." *Proceedings of the world congress on engineering*. 2014.
- 466 [9] Giuffrida, Antonio. "Modelling the performance of a scroll expander for small organic Rankine cycles when
467 changing the working fluid." *Applied Thermal Engineering* 70.1 (2014): 1040-1049.
- 468 [10] Declaye, Sebastian, Sylvain Quoilin, and Vincent Lemort. "Design and experimental Investigation of a
469 small scale Organic Rankine Cycle using a Scroll Expander." (2010).
- 470 [11] Erbaş, Murat, and Atilla Biyikoglu. "Design of low temperature Organic Rankine Cycle and
471 turbine." *Power Engineering, Energy and Electrical Drives (POWERENG)*, 2013 Fourth International
472 Conference on. IEEE, 2013.
- 473 [12] Rahbar, Kiyarash, et al. "Modelling and optimization of organic Rankine cycle based on a small-scale
474 radial inflow turbine." *Energy conversion and management* 91 (2015): 186-198.
- 475 [13] Rahbar, Kiyarash, et al. "Parametric analysis and optimization of a small-scale radial turbine for Organic
476 Rankine Cycle." *Energy* 83 (2015): 696-711.
- 477 [14] Han, Sangjo, JongBeom Seo, and Bum-Seog Choi. "Development of a 200 kW ORC radial turbine for
478 waste heat recovery." *Journal of Mechanical Science and Technology* 28.12 (2014): 5231-5241.
- 479 [15] Cho, S., C. Cho, and C. Kim. "A Study of Cycle Analysis and Turbine Design for Obtaining Small-Scaled
480 Power from the Organic Rankine Cycle Using R245fa." (2013).
- 481 [16] Fiaschi, Daniele, Giampaolo Manfrida, and Francesco Maraschiello. "Thermo-fluid dynamics preliminary
482 design of turbo-expanders for ORC cycles." *Applied energy* 97 (2012): 601-608.
- 483 [17] Harinck, John, et al. "Performance improvement of a radial organic Rankine cycle turbine by means of
484 automated computational fluid dynamic design." *Proceedings of the Institution of Mechanical Engineers, Part A:
485 Journal of Power and Energy* 227.6 (2013): 637-645.
- 486 [18] Sauret, Emilie, and Yuantong Gu. "Three-dimensional off-design numerical analysis of an organic Rankine
487 cycle radial-inflow turbine." *Applied Energy* 135 (2014): 202-211.
- 488 [19] Rahbar K, Mahmoud S, Al-Dadah RK, Moazami N. "One-dimensional and three-dimensional numerical
489 optimization and comparison of single-stage supersonic and dual-stage transonic radial inflow turbines for the
490 ORC. Proceedings of the ASME 2016 Power and Energy Conference, Inpress accepted paper.
- 491 [20] Da Lio, L, Manente, G and Lazzaretto, A. "New efficiency charts for the optimum design of axial flow
492 turbines for organic Rankine cycles". *Energy* 2014; 77, pp. 447- 459.
- 493 [21] Ennil, Ali Bahr, et al. "Minimization of loss in small scale axial air turbine using CFD modeling and
494 evolutionary algorithm optimization." *Applied Thermal Engineering* 102 (2016): 841-848.
- 495 [22] Sauret, Emilie. "Open design of high pressure ratio radial-inflow turbine for academic validation." *ASME
496 Paper No. IMECE2012-88315* (2012).

- 497 [23] Moreau, Aurélien Marsan-Stéphane. "ANALYSIS OF THE FLOW STRUCTURE IN A RADIAL
498 TURBINE."
- 499 [24] Odabae, M., Mohsen Modir Shanechi, and K. Hooman. "CFD Simulation and FE Analysis of a High
500 Pressure Ratio Radial Inflow Turbine." 19AFMC: 19th Australasian Fluid Mechanics Conference. Australasian
501 Fluid Mechanics Society, 2014.
- 502 [25] Tsalicoglou, Isaak, and Bent Phillipsen. "Design of radial turbine meridional profiles using particle swarm
503 optimization." 2nd International Conference on Engineering Optimization. 2010.
- 504 [26] Fu, Lei, et al. "Integrated optimization design for a radial turbine wheel of a 100 kW-class
505 microturbine." *Journal of Engineering for Gas Turbines and Power* 134.1 (2012): 012301.
- 506 [27] Zhang, Qiang, and Chaochen Ma. "Multiple-objective aerodynamic optimization design of a radial air
507 turbine impeller." *Remote Sensing, Environment and Transportation Engineering (RSETE)*, 2011 International
508 Conference on. IEEE, 2011.
- 509 [28] Van den Braembussche, R. A. Optimization of radial impeller geometry. VON KARMAN INST FOR
510 FLUID DYNAMICS RHODE-SAINT-GENESE (BELGIUM), 2006.
- 511 [29]. Mueller, Lasse, Zuheyr Alsalihi, and Tom Verstraete. "Multidisciplinary optimization of a turbocharger
512 radial turbine." *Journal of Turbomachinery* 135.2 (2013): 021022.
- 513 [30] Klein, SA Engineering equation solver. F-chart Software, Middleton, WI; 2013.
- 514 [31] Balje, O. "Turbomachines. A guide to Design, Selection and Theory. JohnWiley & Sons." Inc., New
515 York (1981).
- 516 [32] Rohlik H. E., "Analytical determination of radial inflow turbine design geometry for maximum efficiency,"
517 Tech. Rep. TN D-4384, NASA, Washington, DC, USA, (1968).
- 518 [33] Rogers C., "Mainline Performance Prediction for Radial Inflow Turbine in Small High Pressure Ratio
519 Turbine," VKI Lecture Series 1987-07, (1987).
- 520 [34] Whitfield A. and Baines N., "Design of Radial Turbomachines", JohnWiley & Sons, New York, NY, USA,
521 (1990).
- 522 [35] Moustapha H., Zeleski M. F., Baines N. C., and D. Japikse, "Axial and Radial Turbines", Concepts NREC,
523 White River Junction, Vt, USA, (2003).
- 524 [36] Aungier H., "Turbine Aerodynamics: Axial-Flow and Radial- Flow Turbine Design and Analysis", ASME
525 Press, New York, NY, USA, (2006).
- 526 [37] Dixon, S.L. and Hall C., "Fluid mechanics and thermodynamics of turbomachinery". Butterworth-
527 Heinemann, Oxford, UK (2013).
- 528 [38] Suhrmann, J.F., Peitsch, D., Gugau, M., Heuer, T., and Tomm, U., 2010, "Validation and development of
529 loss models for small size radial turbines." *Proceedings of ASME Turbo Expo 2010: Power for land, sea and
530 Air GT 2010*, Glasgow, UK, Paper No GT (2010)-22666.
- 531 [39] Glassman A.J., "Computer program for design and analysis of radial inflow turbines". NASA TN 8164;
532 (1976).
- 533 [40] Churchill SW. "Friction-factor equation spans all fluid-flow regimes". *Chem Eng* (1977);84:91-2.
- 534 [41] Wilson, David Gordon, and Theodosios Korakianitis. *The design of high-efficiency turbomachinery and
535 gas turbines*. MIT press, 2014.
- 536 [42] Al Jubori A, Al-Dadah RK, Mahmoud S, Khalil KM, Bahr Ennil AS. "Development of efficient small scale
537 axial turbine for solar driven organic Rankine cycle". *Proceedings of ASME Turbo Expo 2016: GT2016*, Seoul,
538 South Korea, paper no GT2016-57845.
- 539 [43] ANSYS 15 CFX-Solver Theory Guide.
- 540 [44] Kim, Jin-Hyuk, et al. "Performance enhancement of axial fan blade through multi-objective optimization
541 techniques." *Journal of Mechanical Science and Technology* 24.10 (2010): 2059-2066.
- 542 [45] Surekha, N., Srinivas Kolla, Deva Raj Ch, and K. Sreekanth. "Optimization of Principal Dimensions of
543 Radial Flow Gas Turbine Rotor Using Genetic Algorithm." *Int. J. Scientific & Engineering Research* 2012;3:1-6.
- 544 [46] McLallin, K.L.; and Haas, J.E., "Experimental Performance and Analysis of 15.04-cm-tip-diameter, Radial-
545 inflow Turbine with Work Factor of 1.126 and Thick Blading". NASA TP-1730, (1980).
- 546 [47] Jones, Anthony C. "Design and test of a small, high pressure ratio radial turbine." ASME 1994
547 International Gas Turbine and Aeroengine Congress and Exposition. American Society of Mechanical
548 Engineers, 1994.

549

550

551

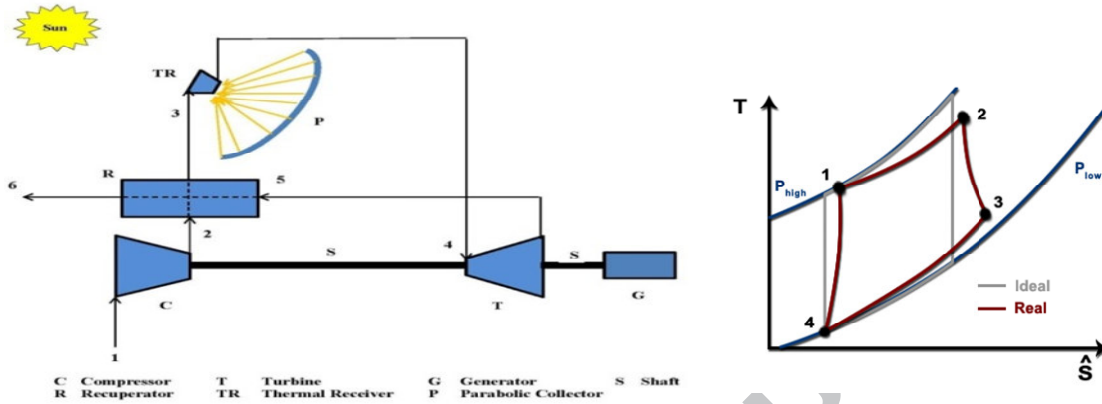
552

553

554

555

556



557

558

559

560

561

562

563

Fig.1. Schematic diagram of CSP-BC system.

Fig. 2. T-S diagram of Brayton cycle.

564

565

566

567

568

569

570

571

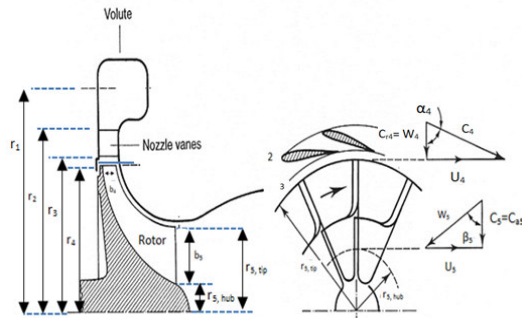


Fig. 3. Schematic view and the meanline velocity triangles of the radial turbine.

572

573

574

575

576

577

578

579

580

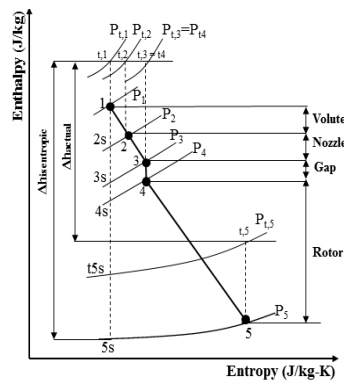


Fig. 4. Enthalpy-entropy diagram of the turbine.

581

582

583

584

585

586

587

588

589

590

591

592

593

594

595

596

597

598

599

600

601

602

603

604

605

606

607

608

609

610

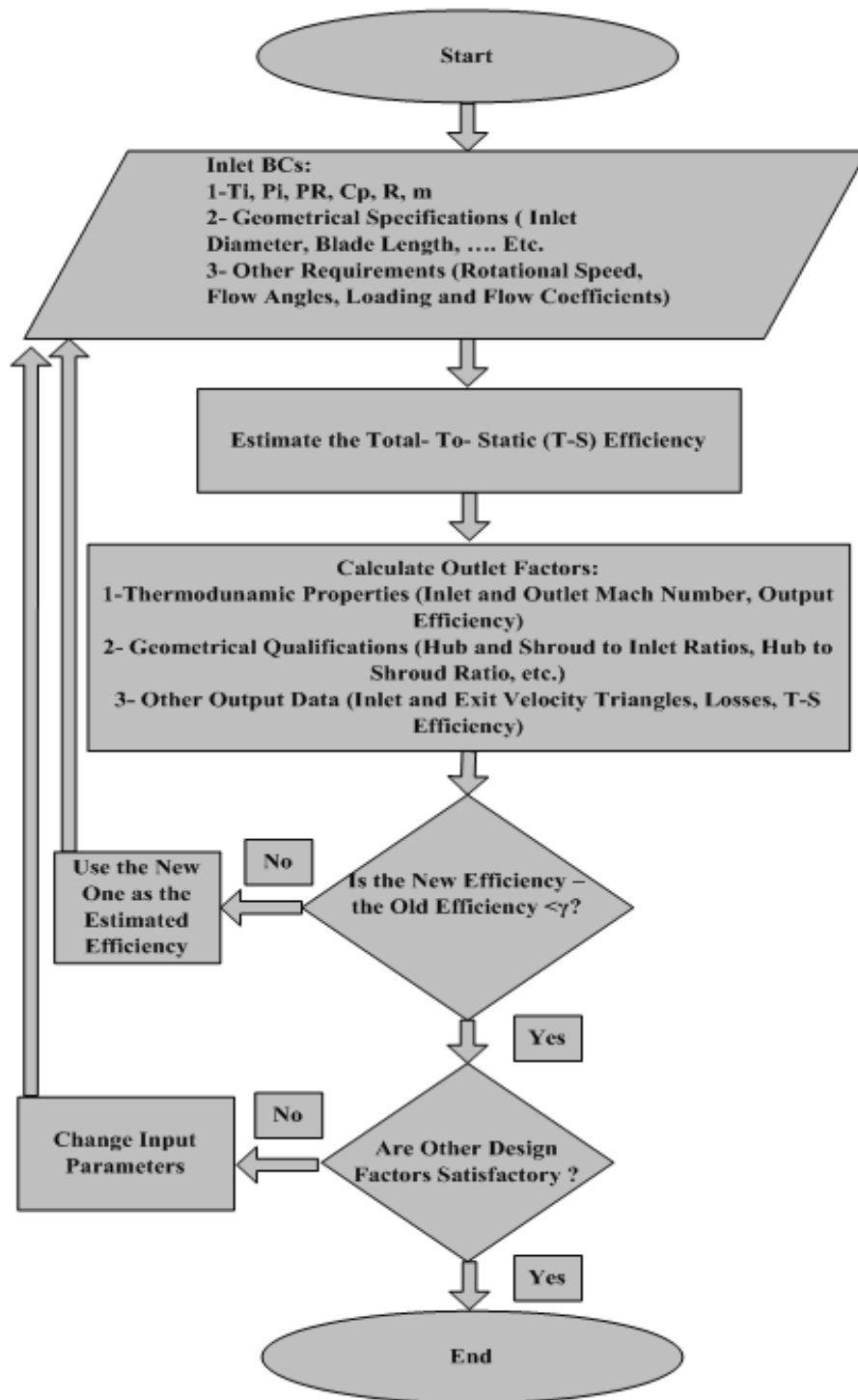


Fig. 5 Algorithm procedure followed for the designed turbines.

611
612
613
614
615
616
617
618
619

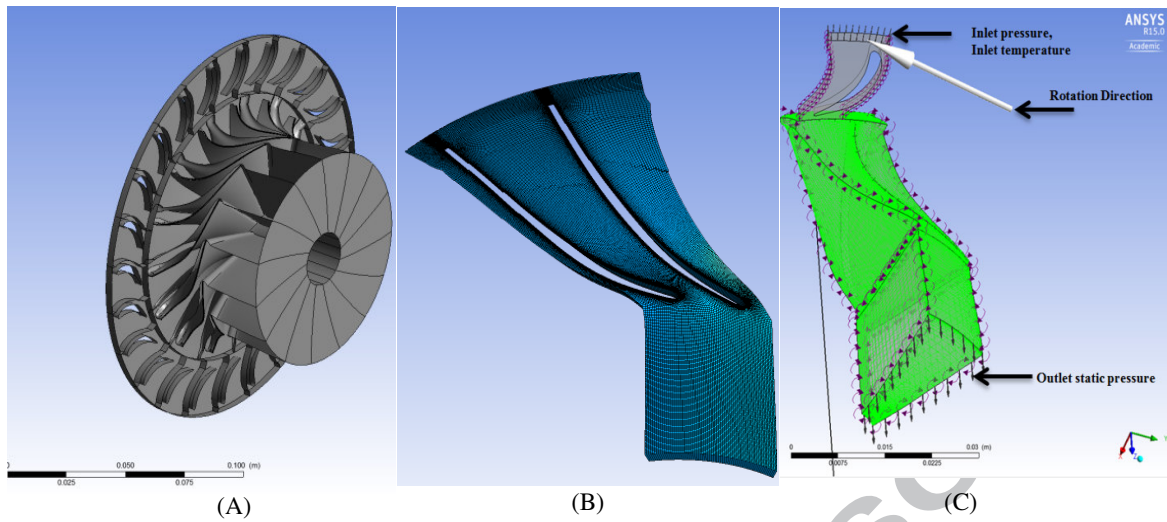


Fig. 6. Three dimensional view of; (A): Radial turbine geometry, (B): 3D mesh generation for the rotor blade and (C): The coupled stator- rotor domain.

621
622
623
624
625
626
627

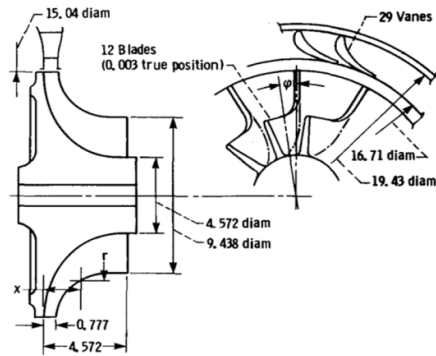


Fig. 7. Schematic view of the radial turbine that used in Ref [47].

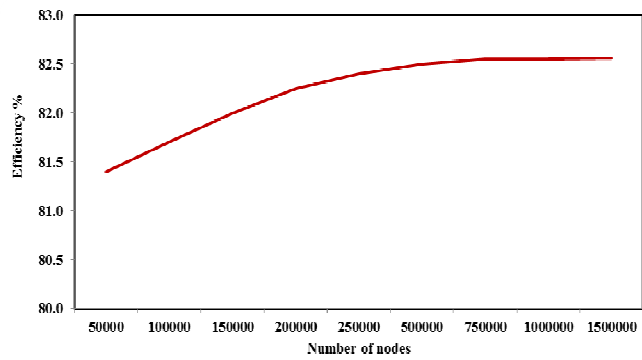


Fig. 8. Mesh sensitivity based on turbine efficiency. Ref [47].

629
630
631
632
633
634
635
636

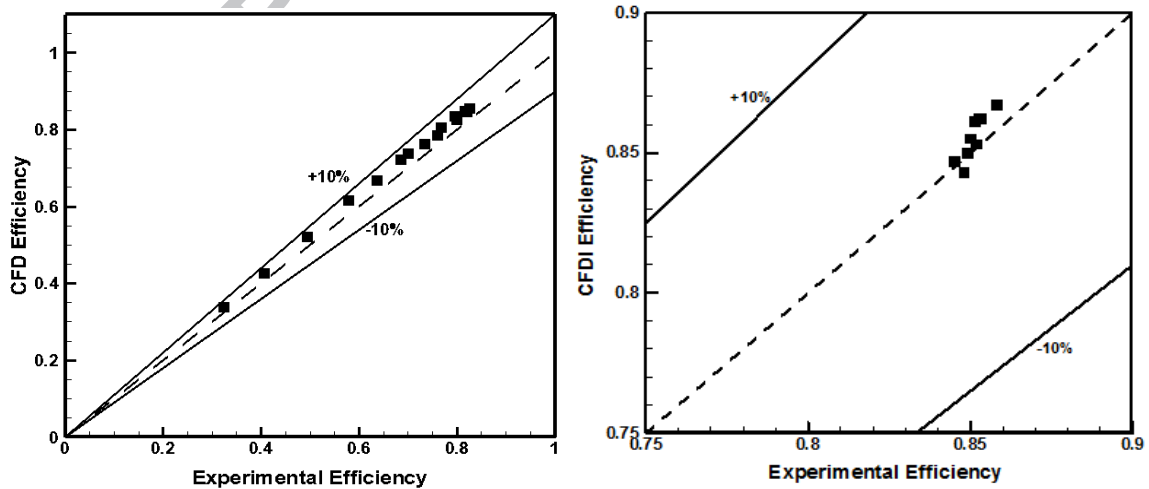


Fig. 9. The efficiency of the current work against two experimental works.

637
638
639

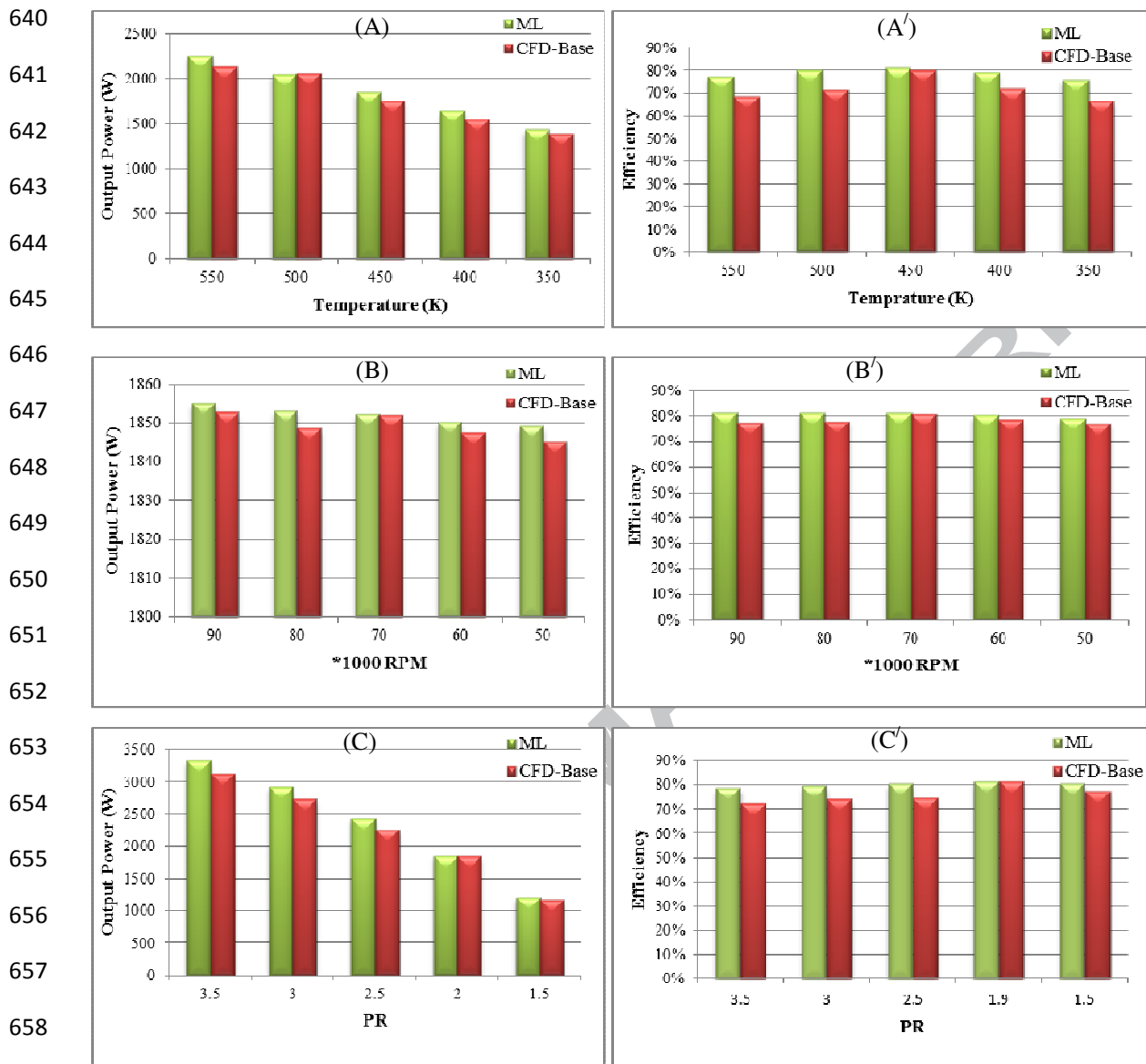


Fig. 10. Comparison between ML and CFD results; efficiency and power output at different: (A) Inlet temp, (B) Rotational speed and (C) Pressure ratio.

668

669

670

671

672

673

674

675

676

677

678

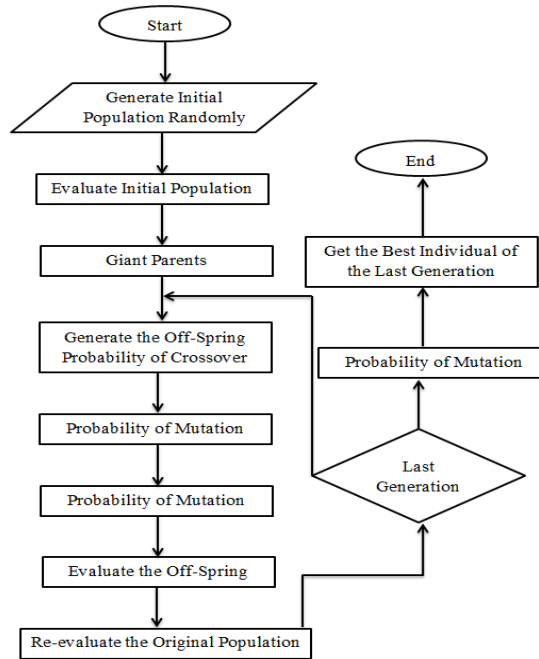


Fig. 11. Genetic algorithm flow chart.

680

681

682

683

684

685

686

687

688

689

690

691

692

693

694

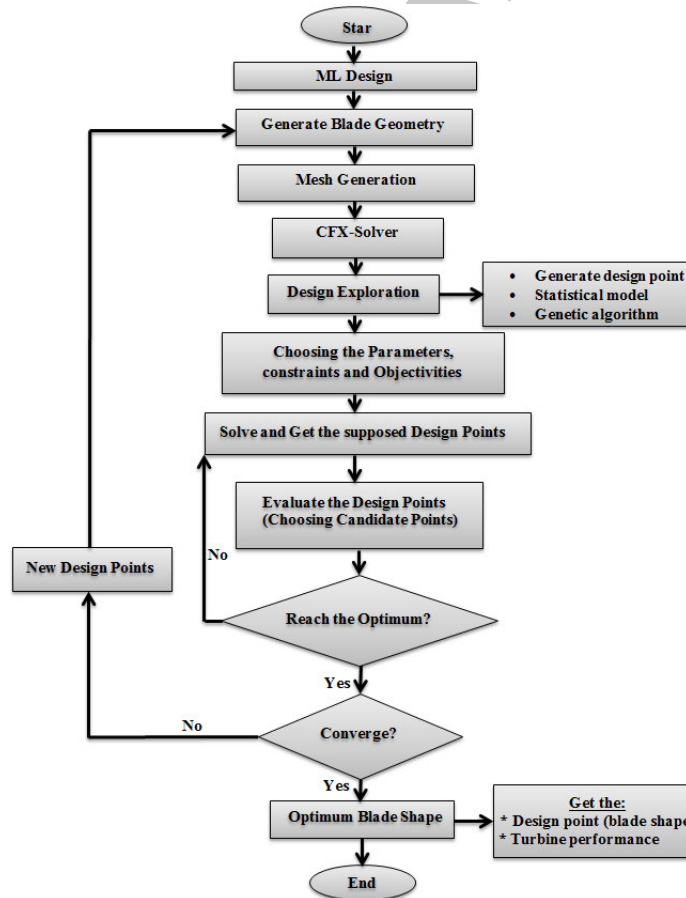


Fig. 12. The procedure followed by the three Dimensional optimization of CFD.

695

696
697
698
699
700
701
702
703
704
705
706
707
708
709
710
711
712
713
714
715
716
717
718
719
720
721
722
723

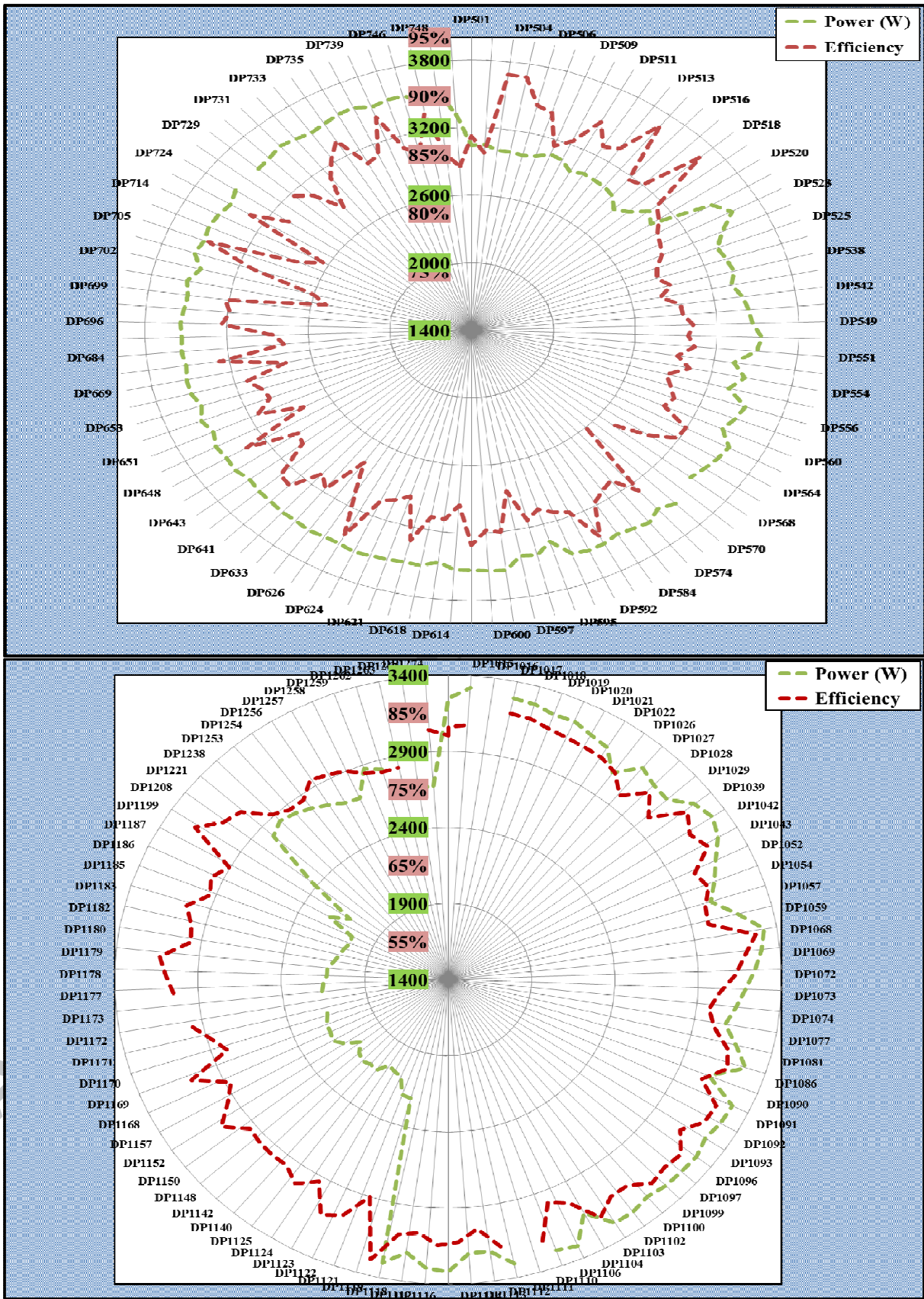


Fig. 13. Modulation of the SSRT efficiency and power output values with some of the investigated design points.

724
725
726
727
728
729
730

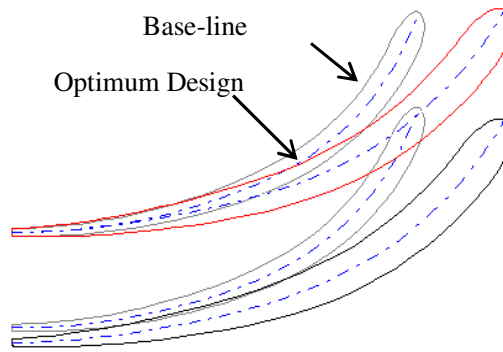


Fig. 14. Comparison between blade geometry at the base-line and optimum

731
732
733
734
735
736
737
738
739
740
741
742
743
744
745
746
747
748
749
750

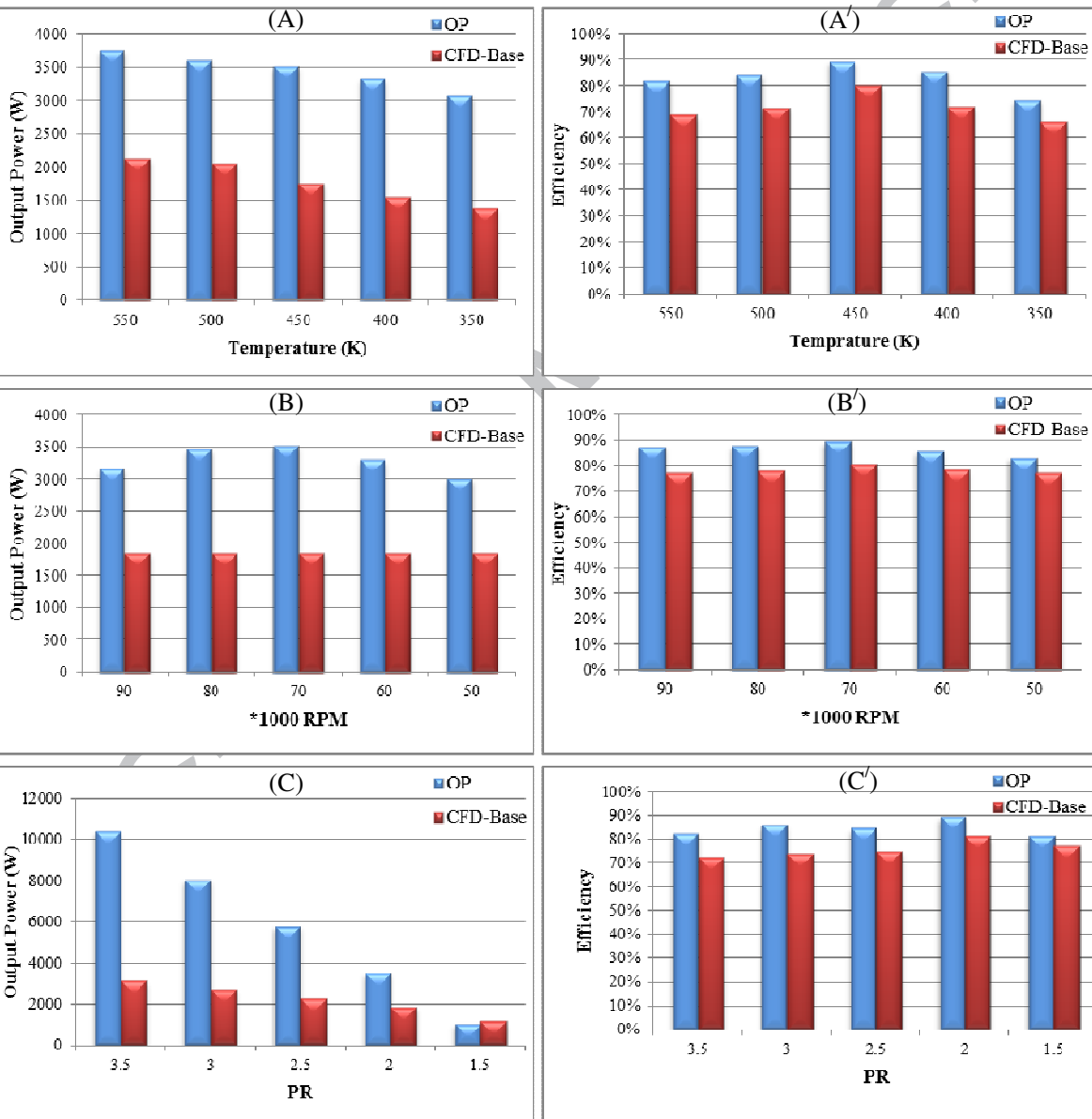


Fig. 15. Comparison between CFD and OP results; efficiency and power output at different: (A) Inlet temp, (B) Rotational speed and (C) Pressure ratio.

751

752

753

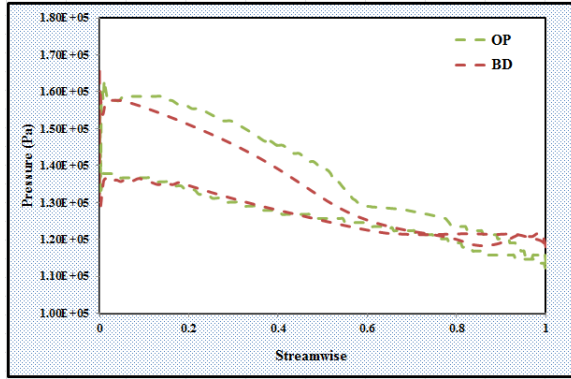
754

755

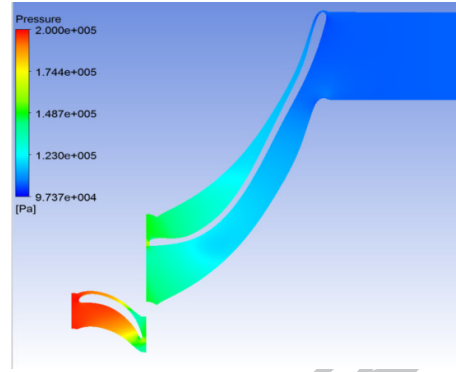
756

757

758



(A)



(B)

759

760

Fig. 16. (A): Pressure distribution of the BL and OP for the rotor blade and (B): Contours of pressure distribution in the stator, rotor and diffuser at 50% span.

761

762

763

764

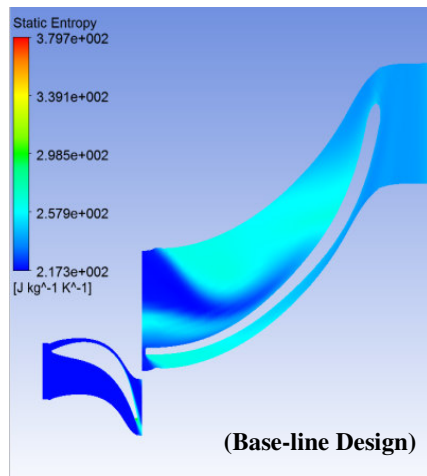
765

766

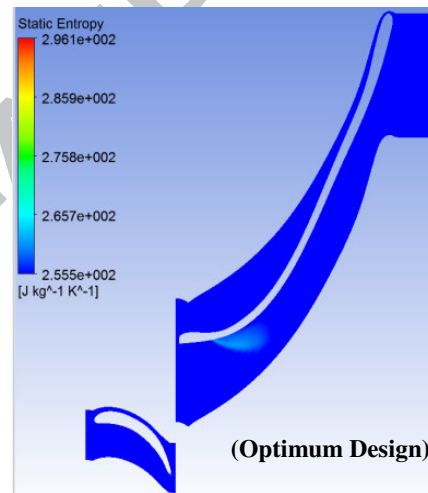
767

768

769



(Base-line Design)



(Optimum Design)

770

771

Fig. 17. Entropy generation at base-line design and optimum design.

772

773

774

775

776

777

778

779

780

781

782

783

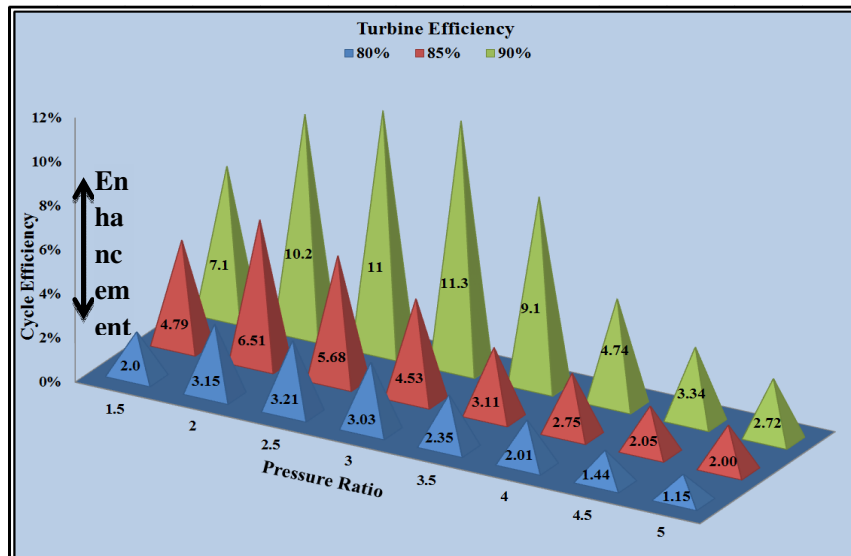
784

785

786

787

788



789

790

791

792

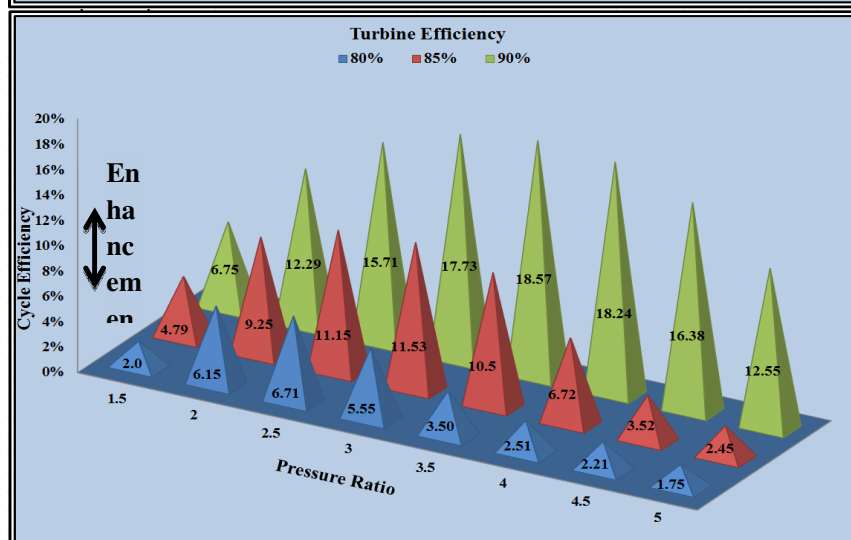
793

794

795

796

797



798

799

800

801

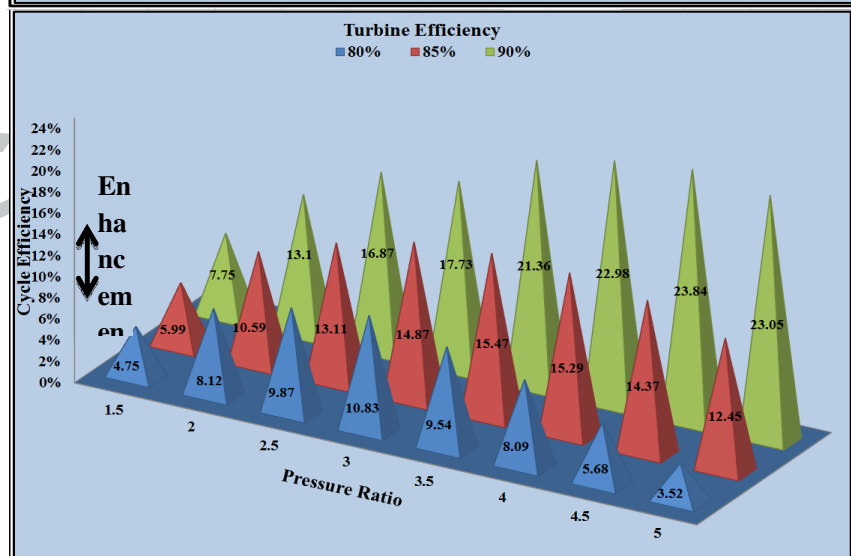
802

803

804

805

806



807

808

Fig. 18. The effect of pressure ratio and turbine efficiency values at inlet temperature of: (A) 450K, (B) 500K and (C) 550K on the cycle efficiency.

809 **Table 1: Input operating conditions of integrated the radial turbine and the Brayton cycle**
 810 **model.**

Parameter	Range/value
Loading coefficient (-)	0.8-1.4
Flow coefficient (-)	0.1-0.5
Shroud _{Exit} /Shroud _{Inlet} (-)	0.8
Hub _{Exit} /Hub _{Inlet} (-)	0.22
Rotational speed (rpm)	50000-90000
Inlet total temperature (K)	450 - 550
Inlet total pressure (bar)	2 -5
Mass flow Rate (kg/sec)	0.03 – 0.05
Working fluids (-)	air
Cp(J/kg K)	1005
Inlet blade velocity (m/s)	253.1
Exit blade velocity (at shroud) (m/s)	202
Inlet relative velocity(m/s)	65.8
Exit relative velocity(m/s)	206.3
Inlet absolute velocity(m/s)	250.5
Exit absolute velocity(m/s)	14.7
Rotor inlet density(kg/m ³)	1.153
Rotor inlet Mach (abs) (-)	0.7
Rotor inlet Enthalpy (J/kg)	109463
Rotor outlet Enthalpy (J/kg)	95288.8
Rotor Enthalpy at the leading edge (J/kg)	107811
Rotor Enthalpy at the trailing edge(J/kg)	87117

811

812

813

Table 2: The meanline characteristics of the SSRT.

Nozzle	Value	Unit	Rotor	Value
Meridional length	12.93	(mm)	Axial clearance	0.4
Blade number	28	(-)	Blade number	15
Tip width	1.7	(mm)	Axial length	11.671
Exit height		(mm)	Tip width	1.7
Inlet absolute flow angle	0	(deg.)	Inlet absolute flow angle	75
Inlet height		(mm)	Inlet height	69.06
Inlet radius	50.43	(mm)	Inlet radius	34.53
Outlet absolute flow angle	75	(deg.)	Inlet relative flow angle	-9
Outlet radius	39.71	(mm)	Outlet shroud radius	27.6
TE thickness	0.4	(mm)	Radial clearance	0.4
Throat area	95	(mm ²)	Throat area	95
Aerofoil area	33.18	(mm ²)	Aerofoil area	25.38
Camber length	17.75	(mm)	Camber length	30.975
Cord length	15.63	(mm)	Cord length	27.82
LE thickness	0.25	(mm)	LE thickness	0.25
Pitch cord Ratio	0.448	(-)	Pitch cord ratio	0.365
Solidity	2.22	(-)	Solidity	3.77
Stagger angle	34.2	(deg.)	Stagger angle	-37.1
		(deg.)	Outlet absolute flow angle	-12.5
		(deg.)	Outlet relative flow angle (hub)	-76.3
		(deg.)	Outlet relative flow angle (root mean square)	-79.3
		(deg.)	Outlet relative flow angle(shroud)	-82.1
		(mm)	Outlet hub radius	7.6
		(mm)	TE thickness	0.4

(mm) Meridional length 22.193

815 **Table 3: The data used for validation as reported in references [46, 47].**

Parameter	Reference 46	Reference 47
Working fluid (-)	Air	Air
Mass flow rate (kg)	0.3311224	0.2313
Inlet temperature (K)	1056.483	322.2
Inlet pressure (bar)	40.02673	1.379
Pressure ratio (-)	5.7	3.255
Rotational speed (rpm)	106588	31456
Output power (kW)	37.285	15.5
Turbine efficiency (%)	87	82.7

816

817 **Table 4: The geometrical data used for validation as reported in references [46, 47].**

Parameter	Value
Rotor inlet diameter (m)	0.1504
Ratio of rotor exit tip to inlet diameters (-)	0.6275
Ratio of rotor exit hub to tip diameters (-)	0.4844
Ratio of stator exit to rotor inlet diameters (-)	1.111
Ratio of stator inlet vane height to rotor inlet diameter (-)	0.0726
Ratio of stator exit bane height to rotor inlet diameter (-)	0.0537
Ratio of stator inlet to stator exit diameters (-)	1.163
Number of stator vanes (-)	29
Number of rotor blades (-)	12
Specific speed (-)	0.46
Blade speed ratio (-)	0.609

818

819 **Table 5: The base-line and optimum design variable from CFD-MOGA optimization.**

Design variables	Baseline	Optimum
Stator no. of blade (-)	32	36
Stator stagger angle (deg.)	33	37.739
Stator TE Beta Angle (deg.)	69	73.70
Rotor no. of blade (-)	13	15
Rotor LE beta angle (deg.)	16.2	-46.3109
Rotor Inlet Flow Angle (deg.)	-58.3	74.03
Rotor Stagger Angle at span 0.0 (deg.)	14.4	-16.8
Rotor Stagger Angle at span 0.5(deg.)	-44.7	-37.1
Rotor Stagger Angle at span 1(deg.)	-64.5	-59.3
Rotator TE beta angle (deg.)	-18.5	-9.9457
Rotor Outlet Flow Angle (deg.)	78.9	83.36
Tip width of rotor (mm)	1.35	2.1
Rotor tip clearance (mm)	0.45	0.33

820

821

822

823 **Highlights:**

824

825 • 1D and 3D CFD analysis for compressed air radial turbine was carried out.

826

827 • Small scale radial turbine with high efficiency.

828

829 • 3D MOGA optimization for the radial turbine was achieved.

830

831 • Enhancing the performance of both the turbine and the solar powered Brayton cycle.

832

833 • Excellent agreement between the current CFD results and two experimental works
834 from literatures.

835

836

837